Research Article | Vol. 29, No. 3 / 1 February 2021 / Optics Express 3490
Optics EXPRESS

InP high power monolithically integrated widely tunable laser and SOA array for hybrid integration

KEITH A. MCKINZIE,[1,*] CONG WANG,[1] ABDULLAH AL NOMAN,[1,2] DAVID L. MATHINE,[3] KYUNGHUN HAN,[1,2] DANIEL E. LEAIRD,[1,2] GLORIA E. HOEFLER,[3] VIKRANT LAL,[3] FRED KISH,[3,4] MINGHAO QI,[1,2] AND ANDREW M. WEINER[1,2]

[1]School of Electrical and Computer Engineering, Purdue University, West Lafayette, IN 47907, USA
[2]Birck Nanotechnology Center, 1205 W State Street, West Lafayette, IN 47907, USA
[3]Infinera Corporation, Sunnyvale, CA 94080, USA
[4]Current affiliation: North Carolina State University, Rayleigh, NC 27695, USA
*kmckinz@purdue.edu

Abstract: We present a monolithic InP-based photonic integrated circuit (PIC) consisting of a widely tunable laser master oscillator feeding an array of integrated semiconductor optical amplifiers that are interferometrically combined on-chip in a single-mode waveguide. We demonstrate a stable and efficient on-chip coherent beam combination and obtain up to 240 mW average power from the monolithic PIC, with 30–50 kHz Schawlow-Townes linewidths and >180 mW average power across the extended C-band. We also explored hybrid integration of the InP-based laser and amplifier array PIC with a high quality factor silicon nitride microring resonator. We observe lasing based on gain from the interferometrically combined amplifier array in an external cavity formed via feedback from the silicon nitride microresonator chip; this configuration results in narrowing of the Schawlow-Townes linewidth to ~3 kHz with 37.9 mW average power at the SiN output facet. This work demonstrates a new approach toward high power, narrow linewidth sources that can be integrated with on-chip single-mode waveguide platforms for potential applications in nonlinear integrated photonics.

1. Introduction

Generation of laser radiation with simultaneously high power and good spatial and spectral mode quality is of longstanding interest. Beam combining approaches that offer the possibility to push beyond the capabilities of single laser emitters have been the subject of sustained investigation [1,2]. In coherent beam combining, light from an array of coherent sources oscillating at a common wavelength interferes constructively to form a single beam, usually in the far-field. For good results this requires control of the relative optical path lengths at a deep subwavelength level, which is technically demanding for radiation in the optical domain. Wavelength combining approaches, in which different array elements provide light at different wavelengths, are also well known. Provided that the wavelengths are appropriately controlled, power at multiple wavelengths can be combined into a single spatial mode using frequency selective elements such as diffraction gratings. Since power is combined incoherently, this approach has the advantage that fine control of the optical phase is not required; however, it is not suitable for narrow linewidth single frequency applications. Beam combining research and development has traditionally targeted free-space applications, such as directed energy, free-space optical communications including deep-space communication, and active optical sensing, e.g., coherent lidar. (One notable exception is wavelength-division multiplexed lightwave communications, in

#413434 https://doi.org/10.1364/OE.413434
Journal © 2021 Received 4 Nov 2020; revised 9 Jan 2021; accepted 11 Jan 2021; published 21 Jan 2021

Optics EXPRESS

which different wavelengths are independently modulated with independent data streams and combined into a single spatial mode for fiber transmission.)

Developments in integrated photonics have given rise to new demands for high power, narrow linewidth sources that can be integrated with on-chip single-mode waveguide platforms. In addition to high spectral efficiency coherent fiber communications and radio-frequency photonics applications, nonlinear integrated photonic applications are of particular relevance. Such applications include wavelength conversion, parametric amplification, microresonator frequency combs, and photon pair generation, as well as chip-scale atom traps. Although such integrated photonics applications generally operate at powers substantially lower than do the free-space applications considered above, nevertheless, the powers required often exceed that available with existing on-chip sources.

Microresonator frequency comb generation, in which continuous-wave pumping of a high quality factor microresonator gives rise to formation of combs of optical frequencies spaced by tens to hundreds of gigahertz, offers a prime example. Such combs arise due to nonlinear wave mixing mediated by the optical Kerr effect and are frequently termed Kerr combs [3,4]. Mode-locked laser frequency combs [5] have had revolutionary impact in optical frequency metrology, spectroscopy and other applications, but are generally too bulky for large scale applications outside the laboratory [5]. Since their observation more than a dozen years ago [6], Kerr combs have been the focus of an intense research effort, in large part due to their potential as a compact and widely deployable frequency comb solution. However, Kerr combs have usually been pumped with external cavity lasers or other off-chip sources, often in conjunction with fiber amplifiers, both to achieve the necessary power and to provide the tunability and narrow linewidth necessary for efficient coupling into the resonant mode. Recently, low noise Kerr comb generation has been achieved by directly coupling a semiconductor gain element to a silicon nitride (SiN) microring resonator [7–9]; such work represents important progress toward truly compact and portable comb systems. Nevertheless, significantly stronger pump powers are still desirable to realize high power comb states, such as those from normal dispersion microresonators [10,11], that can be advantageous for applications such as radio-frequency photonics [12] and high-order coherent communications [13,14]. High power, narrow linewidth pump sources are also advantageous for cascaded electro-optic [15,16] or resonant [17] electro-optic comb generators.

Laser sources for integrated photonics include monolithically integrated lasers in III-V materials platforms, heterogeneously or hybrid integrated III-V lasers for silicon photonics, and rare-earth doped silicon photonic waveguide lasers [18] (the latter require optical pumping via an off-chip source and will not be further considered here). As an example of monolithic integration, arrays of tunable lasers, modulators, power monitors, photodetectors and other elements have been fabricated in indium phosphide to realize transmitter and receiver photonic integrated circuits (PICs) for coherent wavelength division multiplexed fiber communications [19,20]. Alternatively, silicon photonics seeks to bring the advantages of advanced silicon manufacturing infrastructure to photonics applications, but must rely on III-V materials for on-chip light sources since silicon is an indirect bandgap material. This can be achieved either by a heterogeneous integration approach, in which arrays of III-V chips are bonded on silicon and then processed at the wafer scale, or by a hybrid integration approach, in which different dies are first processed, then aligned and attached or bonded onto a common substrate [21,22]. Both the monolithic and III-V silicon approaches feature lasers that can tuned throughout the lightwave C band at power levels of at most a few tens of mW, with high sidemode suppression ratios and relatively narrow linewidths (ca. 100 kHz for monolithic tunable lasers, down to below 1 kHz for III-V silicon lasers incorporating intracavity ring resonator filters). Reference [23] reported an InP reflective semiconductor optical amplifier (R-SOA) butt-coupled to a SiN microring resonator chip, achieving a laser linewidth of 13 kHz with 1.7 mW output power. Reference [24] reported multichip hybrid integration using

Optics EXPRESS

butt-coupling between an silicon microring resonator filter chip and III-V gain chip to form the laser cavity, which is then coupled to a III-V booster amplifier chip, with an impressive 100 mW fiber-coupled power and linewidth below 15 kHz across the C-band.

Substantial effort has been invested in development of monolithic InP devices capable of simultaneous high power and narrow linewidth performance. Monolithic master oscillator power amplifier (M-MOPA) architectures featuring a master laser feeding an amplifier with expanded spatial mode or an amplifier array have yielded diffraction-limited cw output power beyond 1 W into free-space [25]. More recent works have reconsidered amplifier arrays in integrated photonics for coherent beam combination. In one example a monolithic InP device features a DFB laser that splits to feed a four-element amplifier array [26] that outputs >100 mW into free space. The central lobe of the far-field pattern contains 14% of the output; this may be indicative of the challenges inherent to achieving high efficiency coherent beam combination. Reference [27], which represents a much higher level of integration, describes a fully-integrated free-space beam steering chip using hybrid III-V silicon technology. The chip comprises a tunable laser and preamplifier, which is split and directed through an array of channel amplifiers to feed a 32-element surface grating array. The powers in the channel amplifiers are not specified but are expected to be low enough to avoid gain saturation. Coherent beam combining is achieved through far-field propagation, with beam steering implemented in one direction via channel-by-channel phase control and in the orthogonal direction via wavelength tuning and grating diffraction. In contrast to these devices which radiate into free-space, Ref. [28] uses a hybrid InP-SiN platform for coherent beam combining into a single waveguide mode. Two InP reflective SOAs are coherently phased by coupling to a common SiN waveguide that forms part of the laser feedback path. 4 mW of output power is reported, with 92% combining efficiency and 350 kHz linewidth. Another work uses a discrete polarization beam splitter to implement a polarization-diversity amplification scheme, in which orthogonally polarized beams first counterpropagate through a single amplifier chip and are then recombined into a single spatial mode [29].

In this paper we demonstrate a novel monolithic master oscillator – power amplifier utilizing components similar to those available from an InP-based photonic integrated circuit (PIC) foundry process [30]. A preliminary report on this work was presented in [31]. Our PIC comprises a widely tunable laser feeding an array of four semiconductor optical amplifiers which are interferometrically combined on-chip in a single-mode waveguide. Our PIC architecture falls within the monolithic master oscillator power amplifier (M-MOPA) category, but with a design optimized for coherent beam combination into a high-confinement-factor single-mode waveguide [25]. Using an array of integrated phase adjusters, we are able to obtain 240 mW average power with 60 dB sidemode suppression ratio at the 1542 nm peak of the gain spectrum. Average power over 180 mW with >42 dB sidemode suppression ratio is maintained when our M-MOPA is tuned across the extended C-band (1513 nm – 1564 nm). Coherent beam combining shows excellent passive stabilty with a combining efficiency of at least 79%. We also performed measurements of the frequency noise power spectral density for precise determination of the Lorentzian (or Schawlow-Townes) linewidth; we obtain Schawlow-Townes linewidths in the range ~30–50 kHz throughout the tuning range. Finally, we explored the functionality of our PIC after hybrid integration with a high quality factor SiN microresonator chip. Under low drive conditions we are able to demonstrate quasi-continuous tuning and control in the presence of weak reflections from the III-V to SiN interface. Under full current the interferometrically combined SOA array itself lases, in conjunction with an external cavity formed via feedback from the silicon nitride microresonator chip. In this configuration we generate 37.9 mW average power at the SiN output facet and measure an FM noise floor showing ~3 kHz Schawlow-Townes linewidth, at or close to our instrumental sensitivity.

Optics EXPRESS

2. Device structure

The InP-based photonic integrated circuits (PIC) are fabricated using a system on chip PIC integration platform that monolithically integrates high gain active sections and low-loss passive waveguides. The active elements consist of multi-quantum well (MQW) active regions whereas the passive regions (waveguides and MMIs) consist of bulk double heterostructures. Conventional growth-etch-regrowth techniques [20] are used to monolithically integrate the different components of the widely tunable, narrow linewidth master oscillator with an array of SOAs. After the epitaxial (re)growths and front-end wafer fabrication (patterning and etching) are complete, the PIC wafers are subjected to a back-end wafer fabrication process sequence to define the active/passive waveguide and form inter-device and channel–channel electrical isolation, contacts and regions of the active devices. Once the wafer fabrication steps are complete, the wafers are subjected to a die fabrication sequence wherein they are singulated into individual die (via cleaving) and each die is coated with an antireflection coating. The die are subsequently solder die-attached to an AlN carrier, forming a chip-on-carrier (CoC). The CoC were mounted on a customized temperature controlled vacuum chuck with a temperature stability of +/- 0.01 C. A custom optoelectronic probe station was built to permit alignment of an output optical fiber, multiple individual DC probes, and a custom high density probe card. Additionally, a home-built high-density driver was used to provide the required PIC control signals.

The widely tunable master oscillator used was an experimental variation of a DBR-type commercial laser previously described [20] and most recently optimized as a foundry offering [30]. The device featured differentially tuned grating mirrors enabling Vernier tuning over the extended C-band [20] and quasi-continuous tuning over 5 nm and was integrated with an array of SOAs.

In this work we demonstrate coherent combination of four SOAs on a single PIC, although there is no fundamental limit to scaling to a larger number of SOAs. InP PICs are typically realized using a high-confinement-factor integration platform to achieve maximum modal gain for lasers and high efficiency for modulators and photodetectors. Thus, the coherent combination of an SOA array approach was implemented to scale the output power beyond the saturation power of individual SOAs in this integration platform. Three successive PIC designs were explored to optimize the power from the interferometric combination of SOAs. The first PIC featured two SOAs (dual SOA), with the relative phase between each SOA controlled via the drive currents to the individual SOAs. Two dual SOA variants were fabricated and compared; one variant featured two SOAs with single electrodes of constant transverse mode size, while the second variant consisted of two SOAs with a flared optical mode to adiabatically increase then decrease the transverse mode profile in an attempt to boost the SOA saturation power [32]. The latter variant is shown in Fig. 1(a), referred herein as dual SOA with flared electrode design.

The second iteration consisted of four SOAs (quad SOA) as shown in Fig. 1(b). The architecture featured a mix of two SOA pairs: the variant with constant transverse mode and the single electrode flared transverse mode design. The relative phase was again controlled by changing each SOA bias current, as previously shown in master oscillator power amplifier literature [33].

The third iteration integrated thermo-optic phase adjusters with an array of four segmented flared SOAs, shown in Fig. 1(c), called the two electrode flared mode design. The SOA electrode was segmented and flared to control the injected current density across the SOA, and four thermo-optic phase adjusters were used to independently control the phase to achieve coherent combination (ϕ_1, ϕ_2, ϕ_3, ϕ_4) [30,34].

All the designs featured an angled output waveguide with an antireflective coating to suppress reflections from the InP-air interface. Despite high reflection suppression, small reflections that pass through the SOA array are amplified and fed back into the laser. Feedback amplitude as low as −90 dB has been shown to impact lasing coherence and linewidth depending on feedback phase [35,36]. To control the phase from the InP-air interface, on the third iteration a thermo-optic

Optics EXPRESS

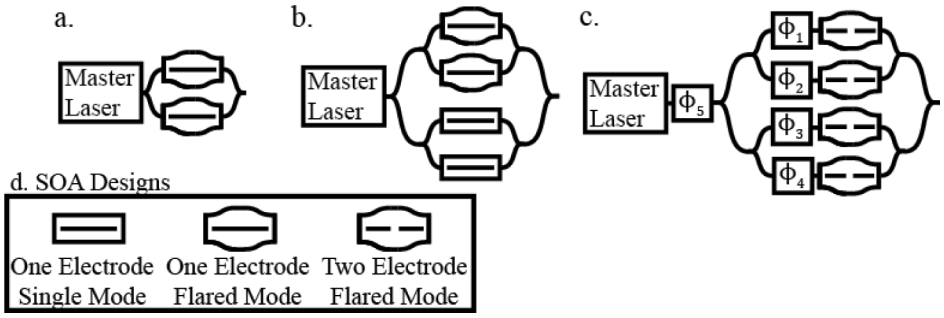

Fig. 1. a. Dual SOA architecture utilizing single electrode SOA variant, b. quad SOA architecture with mixed SOA designs, c. quad SOA architecture with integrated phase adjusters (ϕ_1-ϕ_4) for coherent combination and linewidth control (ϕ_5), d. summary of SOA variants tested.

phase adjuster (ϕ_5) was incorporated between the master laser and the SOA array, yielding linewidth control. We will refer to the ϕ_5 element as an external cavity phase adjuster since it is situated outside the master oscillator laser cavity.

3. Optical power testing

We now report on the optical power performance of the master oscillator – interferometric power amplifier PICs from the third iteration. Detailed results from the first and second iteration are reported in Supplement 1, Sections 1 and 2 respectively, as are aspects of our experimental methodology.

The third generation PICs consisted of four SOAs in the flared mode configuration. Each SOA gain region was segmented into two equal lengths with separate electrodes to improve the spatial control of the carrier density along the length of the SOA device, which simultaneously increases saturation power and reduces noise figure [34]. In addition, the design included integrated thermo-optic phase adjusters inside the nested Mach-Zehnder interferometer to compensate for phase differences between the arms. This prevents power lost due to SOA drive variations without phase adjusters, as discussed in Supplement 1, Section 2. Figure 2 shows the output power for a single SOA (others left open) measured with an integrating sphere, for different currents to the front and back SOA segments. The laser's tuning elements were left open, leaving the laser at 1537 nm instead of the designed gain center of 1542 nm. We show that equal drive to both SOA segments gives the maximum output power, with an estimated single SOA power of ~76 mW; this value is obtained by multiplying the measured power by a factor of four to account for the 6 dB loss that the output of a single SOA encounters in passing through two 3 dB couplers in exiting from the nested interferometers. This represents a 38% increase in SOA output power, compared to the 55 mW maximum per single electrode SOA measured in the 2 SOA PIC design reported in Supplement 1, Section 1. We attribute this increase to control of current density via sectioning of the gain region.

In order to investigate the coherent combination performance of the third generation PICs, the laser is tuned to the center of the gain spectrum (1542 nm), and measurements are performed with various numbers (N) of SOAs excited. The SOAs employed are biased symmetrically (equal current to each electrode); unused SOAs are left open circuited. The thermo-optic phase adjusters were iteratively adjusted for maximum power output, using the algorithm described in the Supplement 1, Section 2. After reaching the maximum power, the phase of one of the thermo-optic phase adjusters was swept in order to observe the interference of one SOA against the *N-1* SOAs that remain coherently combined. We can understand the power scaling with

Optics EXPRESS

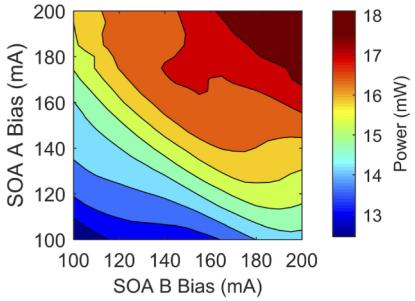

Fig. 2. Measured facet power for the third generation PIC vs. input segment (A) bias and output segment (B) bias. Only a single SOA is excited.

the number of SOAs excited (N) as follows. First, assuming each SOA generates the same output power P_o, ideal power combining yields an output power that scales linearly with N, i.e., $P_{out} = NP_o$. However, each of our SOAs is embedded in an M arm interferometer ($N \leq M$), i.e., one SOA in each of M interferometer arms. Then with one SOA on only, we get an output of P_o/M, where the $1/M$ is the loss that one SOA incurs in going through the interferometer output coupling regions. If we have N out of the M SOAs on and perfectly in phase, then we add N fields and square, so the output power is

$$P_{out} = \frac{N^2 P_o}{M} \tag{1}$$

We see that the output power scales quadratically with the number of SOAs excited inside the M-arm interferometer. When all the SOAs are turned on, we have $N = M$ and obtain the expected $P_{out} = NP_o$. If in a similar way when we have N SOAs turned on, but one is exactly out of phase with all the others ($2 \leq N \leq M$), the resultant output power is given by

$$P_{out} = \frac{(N-2)^2 P_o}{M} \tag{2}$$

For our experiments $M=4$, and the interference contrast (maximum to minimum power ratio) is expected to be 1:0, 9:1, and 4:1, for $N = 2$, 3, and 4, respectively.

Figure 3 shows the measured output power as the SOA phase is varied. In the two SOA case, we measured a 20 dB extinction ratio, with a maximum power of 72.48 mW, showing near balance in the individual SOA contributions (Fig. 3(a)). For three SOAs, the maximum power with coherent combination reached 151 mW, with an extinction ratio of 9.5 dB for equal SOA output powers with 3 out of 4 SOAs powered. For four SOAs, the maximum power was 240 mW, and an extinction of 6.8 dB was measured averaged over the four interference traces which is close to the expected value of 6dB. These results provide evidence of high-quality control of the coherent combination process with the integrated independent DC phase controls. Note that the variations in maximum powers and extinction over the full range of phase shifts is attributed to mechanical drifting of the lensed fiber relative to the chip during the measurement.

Table 1 compares the maximum powers obtained vs. number of SOAs excited (N) to the values predicted for ideal coherent combination from Eq. (1) above. The single SOA power (P_o) was measured with one SOA excited using symmetric current biases of 200 mA per electrode, and the other SOAs open left open. This measurement was performed for each of the four SOAs. The average value and standard deviation between 4 SOAs, 18.98 mW ± 0.89 mW, is reported in Table 1. This number was extrapolated to 2, 3, and 4 SOAs using Eq. (1) to yield the expected power. Roughly we do see the expected N^2 power scaling. However, we note that the actual

Optics EXPRESS

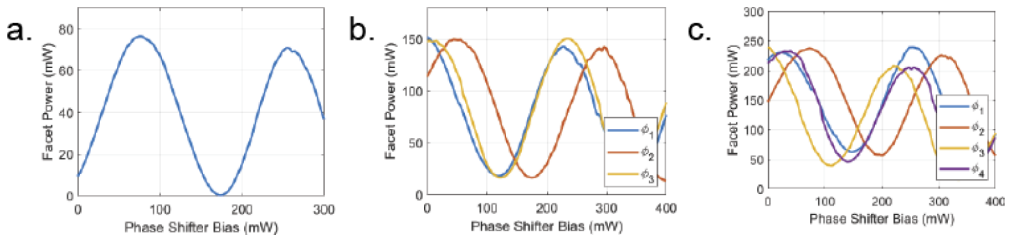

Fig. 3. The representative curves with 3a. 2 SOA, 3b. 3 SOA, and 3c. 4 SOA coherent combination on chip, showing the measured converged iterative power levels.

power for *N=4* is about 21% below the estimated ideal value, which we believe can be attributed to SOA power reduction from local heating of the SOA array.

Table 1. Measured power scaling for the fully combined PIC as a function of the number of SOAs excited (*N*)

Wavelength: 1542 nm	Facet Power (mW)		
N SOAs	Measured	Expected	$P_{Meas}/P_{Expected}$ (%)
1	18.98 ± 0.89	–	–
2	72.48	76	95
3	150.56	171	88
4	240.04	304	79

4. Widely tunable narrow linewidth pump laser

We now present data on the tunability, spectral purity, and linewidth of the tunable laser, both with and without high power amplification. The master laser is a custom variation of a commercially available widely tunable sampled grating tunable distributed feedback laser [20], and we observe similar tuning characteristics shown in Supplement 1, Fig. S3.

Figure 4 shows data on output power and side mode suppression as the laser is coarsely tuned, both with and without amplification. Figure 4(a) shows the spectral performance without amplification (single SOA biased below transparency), measured using an OSA set for 1.2 GHz (0.01 nm) spectral resolution. The laser maintains over 60 dB side mode suppression ratio over the extended C band. Note that the low output powers shown are the result of absorption in the SOA array. Figure 4(b) shows data for the laser output after iterative power combination of the fully biased SOAs. At the center of the gain spectrum (1542 nm), the facet power was 240 mW, and the side mode suppression ratio remained at 60dB even under this full amplification condition as shown in Fig. 4(c).

Next we discuss measurements of the laser linewidth and frequency noise. The master laser's high frequency equivalent linewidth is expected to be of order 200 kHz, similar that of its commercial variant. However, it is well known that feedback at levels as low as −90 dB, e.g., due to reflection from the InP-air interface, can produce linewidth broadening, multimode lasing, or linewidth narrowing depending on the phase of the reflected signal [35,36]. These effects may be more pronounced if there is gain in the feedback path, as is the case here. Using the tunable phase adjuster labeled ϕ_5 in Fig. 1(c), we can maintain and indeed reduce the laser's Schawlow-Townes linewidth even under full amplification conditions. We measured the laser's frequency noise power spectral density (PSD) using a modified delayed self-heterodyne to resolve the Schawlow-Townes linewidth, as detailed in Supplement 1, Sections 4 and 5.

Optics EXPRESS

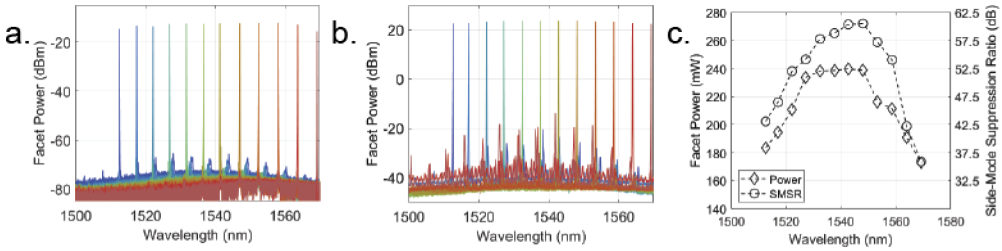

Fig. 4. a. Measured OSA tuning spectra at low power (only a single SOA is on, biased below transparency). 4b. Optical spectra measured with SOAs biased at full current and phased for maximum output power, with phase adjuster ϕ_5 tuned for minimum linewidth. In 4c. the facet power (left, linear scale) and side-mode suppression ratio (SMSR) (right) are shown across the band under high-output power conditions.

We also measured FM noise spectra at a series of discrete wavelengths across the extended C-band, with the SOA array turned on and phased for maximum output power. As before, phase adjuster ϕ_5 was tuned to minimize the frequency noise. The extracted Schawlow-Townes linewidths are plotted in Fig. 5, along with the corresponding OSA spectra (same as Fig. 4(b)). The linewidths fall in the range from ~30 kHz to ~50 kHz. We attribute this narrowing, compared to the unamplified laser's minimum value of ~100 kHz shown in Supplement 1, Fig. S5(b), to optical feedback [20,35,36].

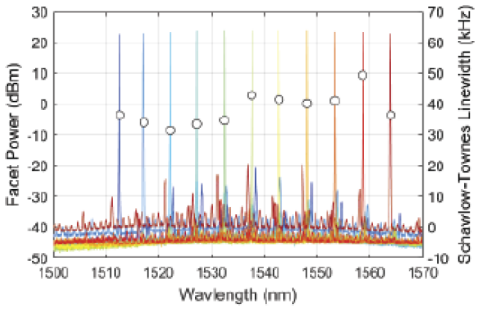

Fig. 5. The reported device's lasing spectra, and measured linewidths.

5. Hybrid integration of InP high power laser and SiN microresonator

Integration of InP laser structures with microresonators in other material systems is of interest for a variety of applications. The most common motivation is to realize silicon photonic microsystems with on-chip light sources. For this purpose a popular approach is to couple an InP gain section to a silicon waveguide section containing one or more tunable ring resonator transmission filters followed by a loop mirror [21,24]. This approach has also been pursued using silicon nitride (SiN) instead of silicon; SiN offers lower loss, resulting in higher quality factor resonators or improved grating lengths, yielding narrower laser linewidths [37,38]. Alternatively, it is possible to use Rayleigh scattering from a microring resonator to provide feedback to the laser gain section. Rayleigh backscattering from ultrahigh-Q whispering gallery mode resonators has been used extensively to realize ultra-narrow linewidth from semiconductor diode lasers [39–42]. Rayleigh backscattering from SiN microring resonators has also been used as the end reflector for an InP semiconductor optical amplifier, resulting in laser oscillation with 2 mW facet power and 13 kHz 3 dB linewidth [23]. Kerr comb generation with stable cavity solitons was achieved via an

Optics EXPRESS

extension of this scheme [7]. Here we report hybrid integration of the tunable InP laser and SOA array with a SiN microring resonator (MRR) chip. Under high power operation feedback from the SiN microresonator chip results in an external cavity that reduces the laser frequency noise, resulting in 37.9 mW facet power with Schawlow-Townes linewidth at or below 3 kHz. We attribute the increased power compared to [23] to the interferometric SOA array which serves as the gain element in this mode of operation.

Three iterations were performed to develop the hybrid integration process, as detailed in Supplement 1, Section 6; several tests were performed after the early assembly campaign to demonstrate functionality. For example, lasers were tuned quasi-continuously in order acquire transmission spectra of the attached MRR chip, using tuning data collected before hybrid integration. Figure 6(a) shows a transmission scan over a 1 nm range, obtained with a single SOA turned on at low bias. The 50 GHz (0.4 nm) free spectral range of the microresonator is clearly observed; a higher order transverse mode is also evident from the data. Note that the slope in the background (off-resonance) power is due to drift in the fiber used to collect the light coupled out of the SiN chip. Figure 6(b) shows a zoom-in of a single resonance. The 3 dB linewidth is ~240 MHz (~2 pm), similar to that measured for the same MRR chip prior to heterogeneous integration. Reflections at the InP-SiN interface also play a role, especially when operating the SOAs for high power. Figure 6(c) shows optical spectrum analyzer data in which the laser spectrum is broadened dramatically by such optical feedback, then restored using the external cavity phase shifter ϕ_5 to the instrumental resolution (~1.2 GHz or 0.01 nm) by applying a phase shifts in increments of $\pi/20$. For higher resolution, we heterodyned the M-MOPA-MRR output with an external cavity reference laser, which yielded a beat note with ~2 MHz linewidth at 10 dB, limited by technical noise of the reference laser. These measurements confirm the functionality of the laser PICs after microring attachment.

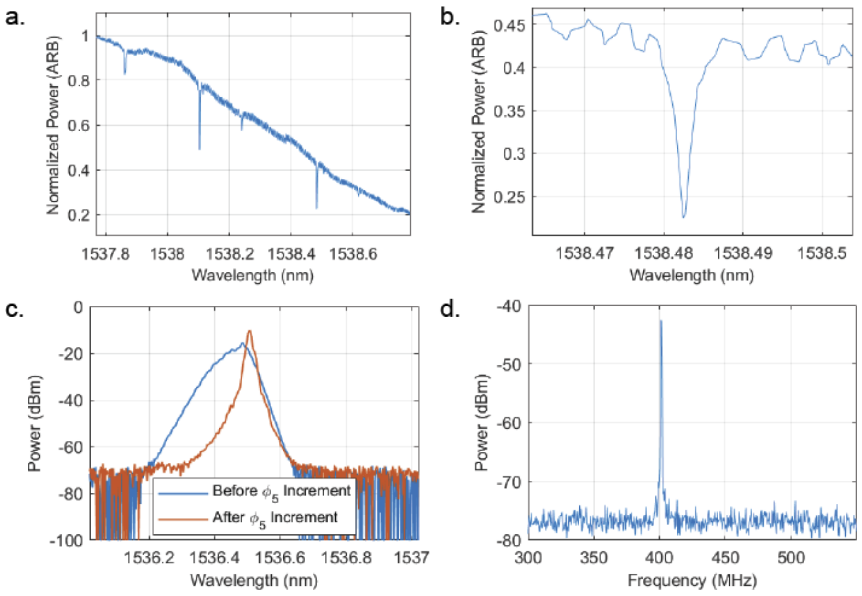

Fig. 6. Functionality tests of early heterogeneously integrated lasers. 6a,b. Transmission spectra of microring resonator measured by tuning the attached laser: 6a. 1 nm tuning range, 6b. zoom-in of a single resonance. 6c. Optical spectrum analyzer data showing compensation of linewidth broadening using the external cavity phase shifter. 6d. Heterodyne beat measurement showing compensation of linewidth broadening.

Optics EXPRESS

The final assembly using the optimized laser PIC was initially tested at low power. The output spectra and optical frequency noise were measured as the laser was tuned discretely from 1513 to 1558 nm in 5 nm increments, with only a single SOA excited weakly. At each tuning step the external cavity phase adjuster was varied to minimize the frequency noise. We observed >50 dB side-mode suppression and high frequency equivalent linewidths in the range 30 to 230 kHz, only slightly degraded compared to the performance without a bonded SiN PIC. However, the behavior was quite different at high power. With all four SOAs driven at maximum current and their respective phase shifters set for optimum coherent combination according to the iterative algorithm described previously, we were unable to achieve single mode lasing controlled by the master laser. On the other hand, we found that we if we turned off the current to the laser gain section, we could obtain stable, high quality laser spectra. Lasing occurred near the peak of the SOA gain spectrum. Our interpretation is that under these conditions the SOA array provided the gain for a laser cavity formed by the tunable laser front mirror (the one closest to the SOAs) and an external cavity resulting either a reflection from the InP-SiN interface or Rayleigh backscattering from the microring resonator. We observed that the lasing spectrum could be shifted slightly by varying the bias on the laser front mirror and cycled between 1542 nm and 1547 nm. This spacing matches the 5 nm mode spacing of the SG-DBR grating. Figure 7(a) shows optical spectra observed for two different currents to the laser front mirror. The side-mode suppression ratio approaches 56 dB, and the optical power is as high as 37.9 mW (estimated facet power just inside the SiN-air interface). We also measured the frequency noise spectrum under this lasing condition at 1542 nm, Fig. 7(b), showing high-stability lasing. The FM noise floor is estimated at 1000 Hz^2/Hz, which corresponds to a Schawlow-Townes linewidth of roughly 3 kHz due to the intersection of the laser's technical noise and oscilloscope's FM noise, indicating a potentially lower Schawlow-Townes linewidth obscured by the laser and oscilloscope's technical noise. Similar FM noise data are observed for 1547 nm lasing. The very low linewidths observed strongly suggest the role of the microring resonator in reducing the frequency noise. Although this was not our original intent, these observations suggest the viability of an interferometrically combined SOA array coupled with a spectrally selective external cavity incorporating a microring resonator as a potential source for applications requiring both ultralow frequency noise and significant power.

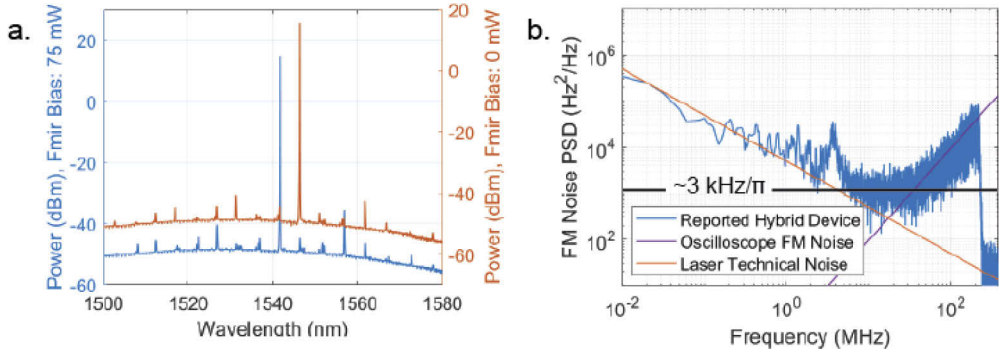

Fig. 7. High power operation of the final laser – MRR assembly. The laser gain section was powered off; the interferometric SOA array provided the gain for laser operation. 7a. Optical power spectra at two different front mirror tuning currents. 7b. Frequency noise spectrum, from which we estimate a maximum ~3 kHz Schawlow-Townes linewidth.

Optics EXPRESS

6. Conclusions

In summary, we report on a monolithic InP photonic integrated circuit based on a foundry compatible process, which is designed to achieve high power into a single-mode waveguide. Our PIC utilizes a monolithic master oscillator – power amplifier (M-MOPA) architecture which incorporates novel coherent on-chip combining of a four-element interferometric semiconductor amplifier array. The optimized PIC yields a maximum on-chip power of 240 mW at 1542 nm, excellent passive stability, and an estimated coherent combination efficiency of 79%. In tuning experiments we observe greater than 180 mW average power across the extended C-band. We also performed measurements of the optical frequency noise spectrum, which allow us to extract the Schawlow-Townes linewidth. Under high power operation we obtain linewidths between 30 kHz and 50 kHz across the full tuning range. These values are a factor of two to three lower than the Schawlow-Townes linewidth (~100 kHz) measured for the master oscillator laser itself, an improvement obtained by adjusting an external cavity optical phase shifter in the presence of weak optical feedback. We also investigated hybrid integration of the monolithic M-MOPA PIC with a high quality factor silicon nitride microring resonator and obtained InP-SiN insertion losses on the order of 5 dB. Under high power operation we observe a new mode of operation in which lasing occurs with the interferometrically combined amplifier array acting as the gain element, with the master laser turned off. Here the laser cavity is formed by the front mirror of the master laser on one side and via feedback from the silicon nitride microresonator chip on the other. In this configuration we observe further narrowing of the Schawlow-Townes linewidth to ~3 kHz, with 37.9 mW average power at the SiN output facet.

Overall our work constitutes a new on-chip coherent beam combining approach toward high power, narrow linewidth sources that can be integrated with on-chip single-mode waveguide platforms for a variety of potential applications. Our experiments demonstrate coherent beam combining with both high efficiency and intrinsic phase stability. This approach can also be scaled to additional on-chip amplifier elements provided that the thermal reduction of SOA output power is appropriately controlled. In addition to coherent fiber communications, radio-frequency photonics and lidar, such on-chip high power, narrow linewidth sources may be important for nonlinear integrated photonics applications, such as wavelength conversion, microresonator frequency combs, parametric amplification, photon pair generation, and chip-scale atom traps.

Funding. Defense Advanced Research Projects Agency (W31P40-13-1-0018); National Defense Science and Engineering Graduate.

Acknowledgements. We would like to acknowledge Mohammed S. Alshaykh for discussions and Matthew Swabey for help designing drive electronics.

Disclosures. GEH: Infinera Corporation, Sunnyvale CA, 94080, USA (E,I), VL: Infinera Corporation, Sunnyvale CA, 94080, USA, (E,I), FK: Infinera Corporation, Sunnyvale CA, 94080, USA (I,S).

Supplemental document. See Supplement 1 for supporting content (submitted: 10/27/2020 3:38:37 PM; revised: 01/09/2020).

References

1. T. Y. Fan, "Laser beam combining for high-power, high-radiance sources," IEEE J. Sel. Top. Quantum Electron. **11**(3), 567–577 (2005).
2. A. Brignon, ed., *Coherent Laser Beam Combining* (Wiley-VCH, 2013).
3. A. Pasquazi, M. Peccianti, L. Razzari, D. J. Moss, S. Coen, M. Erkintalo, Y. K. Chembo, T. Hansson, S. Wabnitz, P. Del'Haye, X. Xue, A. M. Weiner, and R. Morandotti, "Micro-combs: A novel generation of optical sources," Phys. Rep. **729**, 1–81 (2018).
4. A. L. Gaeta, M. Lipson, and T. J. Kippenberg, "Photonic-chip-based frequency combs," Nat. Photonics **13**(3), 158–169 (2019).
5. J. Ye and S. T. Cundiff, eds., *Femtosecond Optical Frequency Comb: Principle, Operation, and Applications* (Springer, 2005).
6. P. Del'Haye, A. Schliesser, O. Arcizet, T. Wilken, R. Holzwarth, and T. J. Kippenberg, "Optical frequency comb generation from a monolithic microresonator," Nature **450**(7173), 1214–1217 (2007).

Optics EXPRESS

7. B. Stern, X. Ji, Y. Okawachi, A. L. Gaeta, and M. Lipson, "Battery-operated integrated frequency comb generator," Nature **562**(7727), 401–405 (2018).
8. A. S. Raja, A. S. Voloshin, H. Guo, S. E. Agafonova, J. Liu, A. S. Gorodnitskiy, M. Karpov, N. G. Pavlov, E. Lucas, R. R. Galiev, A. E. Shitikov, J. D. Jost, M. L. Gorodetsky, and T. J. Kippenberg, "Electrically pumped photonic integrated soliton microcomb," Nat. Commun. **10**(1), 1–8 (2019).
9. B. Shen, L. Chang, J. Liu, H. Wang, Q.-F. Yang, C. Xiang, R. N. Wang, J. He, T. Liu, W. Xie, J. Guo, D. Kinghorn, L. Wu, Q. X. Ji, T. J. Kippenberg, K. Vahala, and J. E. Bowers, "Integrated turnkey soliton microcombs," Nature **582**(7812), 365–369 (2020).
10. X. Xue, Y. Xuan, Y. Liu, P.-H. Wang, S. Chen, J. Wang, D. E. Leaird, M. Qi, and A. M. Weiner, "Mode-locked dark pulse Kerr combs in normal-dispersion microresonators," Nat. Photonics **9**(9), 594–600 (2015).
11. X. Xue, P.-H. Wang, Y. Xuan, M. Qi, and A. M. Weiner, "Microresonator Kerr frequency combs with high conversion efficiency," Laser Photonics Rev. **11**(1), 1600276 (2017).
12. M. S. Alshaykh, J. D. McKinney, and A. M. Weiner, "Radio-Frequency Signal Processing Using Optical Frequency Combs," IEEE Photonics Technol. Lett. **31**(23), 1874–1877 (2019).
13. P. Marin-Palomo, J. N. Kemal, M. Karpov, A. Kordts, J. Pfeifle, M. H. P. Pfeiffer, P. Trocha, S. Wolf, V. Brasch, M. H. Anderson, R. Rosenberger, K. Vijayan, W. Freude, T. J. Kippenberg, and C. Koos, "Microresonator-based solitons for massively parallel coherent optical communications," Nature **546**(7657), 274–279 (2017).
14. A. Fülöp, M. Mazur, A. Lorences-Riesgo, ÓB Helgason, P.-H. Wang, Y. Xuan, D. E. Leaird, M. Qi, P. A. Andrekson, A. M. Weiner, and V. Torres-Company, "High-order coherent communications using mode-locked dark-pulse Kerr combs from microresonators," Nat. Commun. **9**(1), 1598 (2018).
15. A. J. Metcalf, V. Torres-Company, D. E. Leaird, and A. M. Weiner, "High-power broadly tunable electrooptic frequency comb generator," IEEE J. Sel. Top. Quantum Electron. **19**(6), 231–236 (2013).
16. N. Andriolli, T. Cassese, M. Chiesa, C. De Dios, and G. Contestabile, "Photonic integrated fully tunable comb generator cascading optical modulators," J. Lightwave Technol. **36**(23), 5685–5689 (2018).
17. M. Zhang, B. Buscaino, C. Wang, A. Shams-Ansari, C. Reimer, R. Zhu, J. M. Kahn, and M. Lončar, "Broadband electro-optic frequency comb generation in a lithium niobate microring resonator," Nature **568**(7752), 373–377 (2019).
18. N. Li, P. Purnawirman, Z. Su, E. S. Magden, P. T. Callahan, K. Shtyrkova, M. Xin, A. Ruocco, C. Baiocco, E. P. Ippen, F. X. Kärtner, J. D. B. Bradley, D. Vermeulen, and M. R. Watts, "High-power thulium lasers on a silicon photonics platform," Opt. Lett. **42**(6), 1181–1184 (2017).
19. F. Kish, V. Lal, P. Evans, S. W. Corzine, M. Ziari, T. Butrie, M. Reffle, H.-S. Tsai, A. Dentai, J. Pleumeekers, M. Missey, M. Fisher, S. Murthy, R. Salvatore, P. Samra, S. Demars, N. Kim, A. James, A. Hosseini, P. Studenkov, M. Lauermann, R. Going, M. Lu, J. Zhang, J. Tang, J. Bostak, T. Vallaitis, M. Kuntz, D. Pavinski, A. Karanicolas, B. Behnia, D. Engel, O. Khayam, N. Modi, M. R. Chitgarha, P. Mertz, W. Ko, R. Maher, J. Osenbach, J. T. Rahn, H. Sun, K.-T. Wu, M. Mitchell, and D. Welch, "System-on-Chip Photonic Integrated Circuits," IEEE J. Sel. Top. Quantum Electron. **24**(1), 1–20 (2018).
20. V. Lal, J. Summers, N. Kim, S. W. Corzine, P. Evans, M. Lauermann, A. Nguyen, A. Hosseini, M. Lu, J. T. Rahn, M. R. Chitgarha, J. Zhang, J. Osenbach, T. Vallaitis, P. Samra, C. Park, M. Kuntz, J. Tang, C. Tsai, H. Sun, R. Schmogrow, D. Pavinski, B. Behnia, P. Mertz, T. Butrie, K. T. Wu, M. Mitchell, M. Ziari, M. Reffle, D. Welch, and F. Kish, "Extended C-Band Tunable Multi-Channel InP-Based Coherent Transmitter PICs," J. Lightwave Technol. **35**(7), 1320–1327 (2017).
21. T. Komljenovic, M. Davenport, J. Hulme, A. Y. Liu, C. T. Santis, A. Spott, S. Srinivasan, E. J. Stanton, C. Zhang, and J. E. Bowers, "Heterogeneous silicon photonic integrated circuits," J. Lightwave Technol. **34**(1), 20–35 (2016).
22. M. A. Tran, D. Huang, and J. E. Bowers, "Tutorial on narrow linewidth tunable semiconductor lasers using Si/III-V heterogeneous integration," APL Photonics **4**(11), 111101 (2019).
23. B. Stern, X. Ji, A. Dutt, and M. Lipson, "Compact narrow-linewidth integrated laser based on low-loss silicon nitride ring resonator," Opt. Lett. **42**(21), 4541–4544 (2017).
24. N. Kobayashi, K. Sato, M. Namiwaka, K. Yamamoto, S. Watanabe, T. Kita, H. Yamada, and H. Yamazaki, "Silicon Photonic Hybrid Ring-Filter External Cavity Wavelength Tunable Lasers," J. Lightwave Technol. **33**(6), 1241–1246 (2015).
25. D. F. Welch and D. G. Mehuys, "High-power coherent, semiconductor laser, master oscillator power amplifiers and amplifier arrays," in *Diode Laser Arrays*, D. Botez and D. R. Scifres, eds. (Cambridge University, 1994), pp. 72–122.
26. L. Hou and J. H. Marsh, "1.55-μm distributed feedback laser monolithically integrated with amplifier array," Opt. Lett. **40**(2), 213–216 (2015).
27. J. C. Hulme, J. K. Doylend, M. J. R. Heck, J. D. Peters, M. L. Davenport, J. T. Bovington, L. A. Coldren, and J. E. Bowers, "Fully integrated hybrid silicon two dimensional beam scanner," Opt. Express **23**(5), 5861–5874 (2015).
28. Y. Zhu and L. Zhu, "Integrated single frequency, high power laser sources based on monolithic and hybrid coherent beam combining," IEEE J. Sel. Top. Quantum Electron. **24**(6), 1–8 (2018).
29. K. Morito and S. Tanaka, "Record high saturation power (+22 dBm) and low noise figure (5.7 dB) polarization-insensitive SOA module," IEEE Photonics Technol. Lett. **17**(6), 1298–1300 (2005).
30. G. E. Hoefler, Y. Zhou, M. Anagnosti, A. Bhardwaj, P. Abolghasem, A. James, S. Luna, P. Debackere, A. Dentai, T. Vallaitis, P. Liu, M. Missey, S. Corzine, P. Evans, V. Lal, M. Ziari, D. Welch, F. Kish, J. S. Suelzer, P. S. Devgan, and

Optics EXPRESS

N. G. Usechak, "Foundry Development of System-On-Chip InP-Based Photonic Integrated Circuits," IEEE J. Sel. Top. Quantum Electron. **25**(5), 1–17 (2019).
31. K. A. McKinzie, C. Wang, A. Al Noman, D. L. Mathine, K. Han, D. E. Leaird, M. Anagnosti, V. Lal, G. E. Hoefler, F. Kish, M. Qi, and A. M. Weiner, "Heterogeneously Integrated InP Widely Tunable Laser and SiN Microring Resonator for Integrated Comb Generation," in 2018 Conference on Lasers and Electro-Optics (CLEO) (2018), pp. 1–2.
32. J. W. Raring, E. J. Skogen, M. L. Mašanović, S. P. Denbaars, and L. A. Coldren, "Demonstration of high saturation power/high gain SOAs using quantum well intermixing based integration platform," Electron. Lett. **41**(24), 1345–1346 (2005).
33. S. M. Redmond, K. J. Creedon, J. E. Kansky, S. J. Augst, L. J. Missaggia, M. K. Connors, R. K. Huang, B. Chann, T. Y. Fan, G. W. Turner, and A. Sanchez-Rubio, "Active coherent beam combining of diode lasers," Opt. Lett. **36**(6), 999–1001 (2011).
34. T. Motaweh, P. Morel, A. Sharaiha, R. Brenot, A. Verdier, and M. Guegan, "Wideband Gain MQW-SOA Modeling and Saturation Power Improvement in a Tri-Electrode Configuration," J. Lightwave Technol. **35**(10), 2003–2009 (2017).
35. R. W. Tkach and A. R. Chraplyvy, "Regimes of feedback effects in 1. 5-μm distributed feedback lasers," J. Lightwave Technol. **4**(11), 1655–1661 (1986).
36. S. Donati and R.-H. Horng, "The Diagram of Feedback Regimes Revisited," IEEE J. Sel. Top. Quantum Electron. **19**(4), 1500309 (2013).
37. K.-J. Boller, A. van Rees, Y. Fan, J. Mak, R. E. M. Lammerink, C. A. A. Franken, P. J. M. van der Slot, D. A. I. Marpaung, C. Fallnich, J. P. Epping, R. M. Oldenbeuving, D. Geskus, R. Dekker, I. Visscher, R. Grootjans, C. G. H. Roeloffzen, M. Hoekman, E. J. Klein, A. Leinse, and R. G. Heideman, "Hybrid Integrated Semiconductor Lasers with Silicon Nitride Feedback Circuits," Photonics **7**(1), 1–33 (2019).
38. C. Xiang, W. Jin, J. Guo, J. D. Peters, M. J. Kennedy, J. Selvidge, P. A. Morton, and J. E. Bowers, "Temperature stable, narrow linewidth heterogeneously integrated semiconductor laser with Si3N4 cavity," in CLEO: Science and Innovations (2020), p. STu3M.6.
39. W. Liang, V. S. Ilchenko, A. A. Savchenkov, A. B. Matsko, D. Seidel, and L. Maleki, "Whispering-gallery-mode-resonator-based ultranarrow linewidth external-cavity semiconductor laser," Opt. Lett. **35**(16), 2822–2824 (2010).
40. V. S. Ilchenko, E. Dale, W. Liang, J. Byrd, D. Eliyahu, A. A. Savchenkov, A. B. Matsko, D. Seidel, and L. Maleki, "Compact tunable kHz-linewidth semiconductor laser stabilized with a whispering-gallery mode microresonator," in *Proc. SPIE* 7913, 79131G (2011).
41. Y. Li, Y. Zhang, H. Chen, S. Yang, and M. Chen, "Tunable Self-Injected Fabry-Perot Laser Diode Coupled to an External High-Q Si 3 N 4 /SiO 2 Microring Resonator," J. Lightwave Technol. **36**(16), 3269–3274 (2018).
42. A. Gil-Molina, O. Westreich, Y. Antman, X. Ji, A. L. Gaeta, and M. Lipson, "Robust Hybrid III-V/Si 3 N 4 Laser with kHz-Linewidth and GHz-Pulling Range," in 2020 Conference on Lasers and Electro-Optics (CLEO) (2020), pp. 1–2.